ACS Photonics

pubs.acs.org/journal/apchd5

Article

Atom–Photon Interactions in Atomic Cladded Waveguides: Bridging Atomic and Telecom Technologies

Roy Zektzer, Eliran Talker, Yefim Barash, Noa Mazurski, Liron Stern, and Uriel Levy*

Cite This: https://dx.doi.org/10.1021/acsphotonics.0c01895

Read Online

ACCESS | Metrics & More | Article Recommendations | Supporting Information

ABSTRACT: Accurate and stable frequency sources can be realized by locking lasers to well-known transitions between energy levels in isolated quantum systems such as alkali atoms. Unfortunately, current implementations of such frequency standards typically involve bulky optical setups and discrete optical components. Furthermore, the common transitions of alkali atoms are in the near-infrared, hindering their use as frequency references in the telecom regime. Our current work is focused on mitigating these deficiencies. In particular, we demonstrate the design, fabrication, and experimental characterization of an on-chip telecom frequency reference that is based on a ladder transition of rubidium atoms integrated with nanoscale optical waveguides. These atomic cladded waveguides are implemented in a serpentine geometry in order to optimize the chip area and maximize the interaction of light with the alkali atoms. Following its fabrication, the device is used to stabilize a telecom laser around a 1.5 μm wavelength to a precision better than 200 kHz at ∼250 s. Moreover, in spite of the fact that the natural lifetime of the excited state of the atom corresponding to only a few megahertz line widths, the nanoscale confinement of the optical mode dictates ultrashort interaction times and extreme photonic energy densities allowing us to demonstrate low power and faster (∼200 MHz) all-optical modulation of a near-infrared light with a telecom light. The results presented in this paper push forward the efforts toward fully integrated chip-scale stabilization system and provide an extremely efficient link between atomic based devices and silicon photonics platform in the telecom.

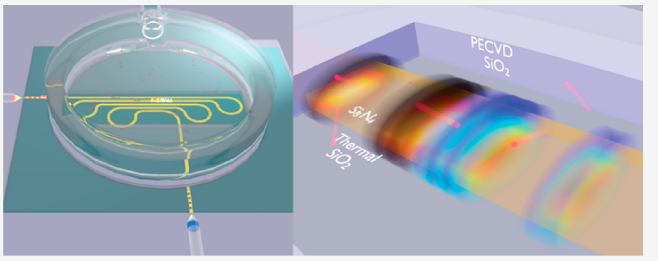

KEYWORDS: *integrated photonics, waveguides, atomic physics, frequency reference*

With a motivation to directly connect microprocessing units to optical fibers, and the rise of data centers as a major customer for large data traffic, silicon photonics was established and developed very rapidly over the last couple of decades.[1−4] Today, as a mature technology, silicon photonics[5] enables the implementation of a large plethora of devices, including low loss waveguides,[6−9] photodetectors,[10−12] modulators,[13−16] demultiplexers,[17] and mode converters[18] to name a few. The merits of such devices, alongside the capability to integrate them using a unified silicon platform, make silicon photonics the technology of choice not only for telecommunication but also for many other use cases. And indeed, we recently observed a major effort to place micro- and nanoscale metrology-based devices on a chip, including for example temperature sensors,[19] short time frequency stabilization devices,[20] beam position sensors,[21] and gyroscopes.[22,23] The recent progress in chip-scale microcombs[24−28] offers a new avenue for metrology on a chip and coherent wavelength division multiplexing systems.[27,29,30] However, while the optical comb offers densely and evenly spaced (in frequency) coherent sources at the telecom, it still needs to be stabilized to a known frequency reference in order to prevent frequency drift and provide the required frequency precision and accuracy.[24]

Atoms such as rubidium (Rb) and cesium (Cs) have been studied extensively over the years due their application in quantum technology,[31] metrology,[25] and sensing.[32] The known energy structure results in accurate and stable optical transitions that the laser's frequency can be stabilized to. Typically, frequency references rely on bulky atomic cells and free-space optics. However, over the past few years, there is a rapidly growing interest in the science and technology of miniaturized atomic cells, creating new opportunities for miniaturized and integrated frequency references, optical clocks, and sensors. Devices such as tapered fibers,[33] hollow-core waveguides[34] and microfabricated cells.[35] In the interest of seizing the huge opportunity presented by silicon photonics of establishing atomic-based stable frequency sources, sensors, and quantum memories on a chip, the atomic cladded waveguides (ACWGs) were demonstrated.[36−39] The ACWG

Received: December 14, 2020

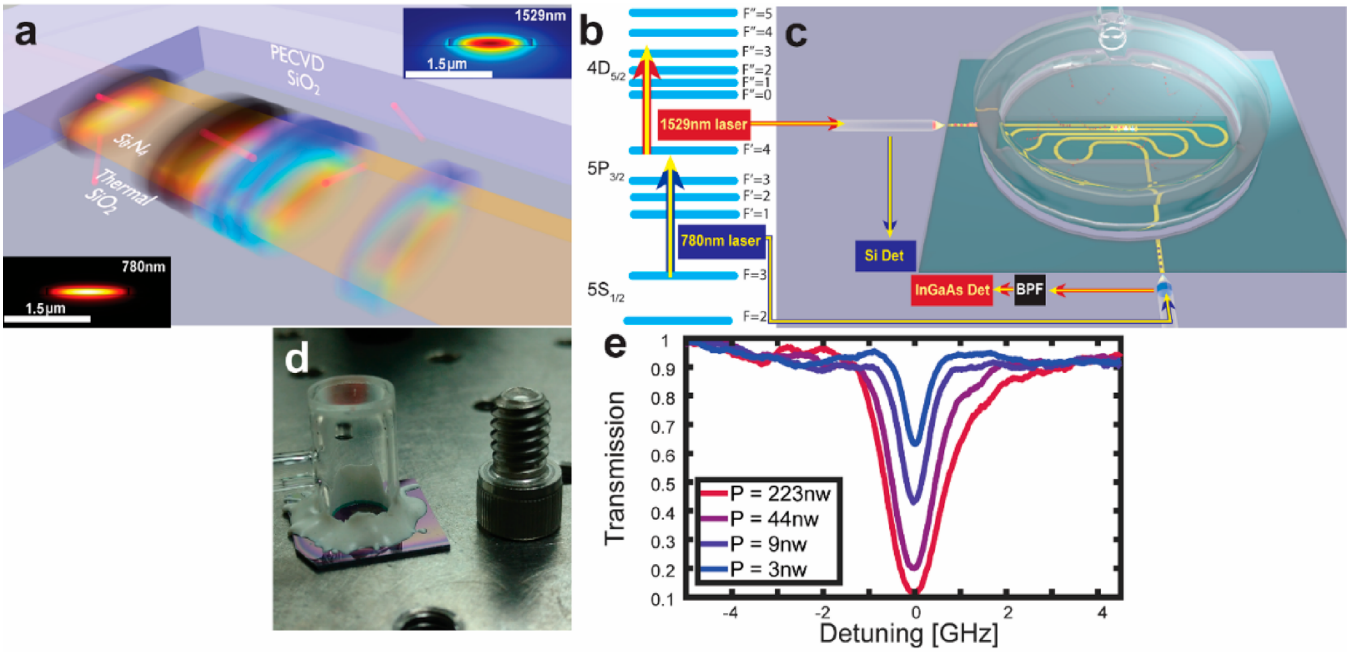

Figure 1. (a) Schematic of the interaction region: The optical modes propagate along the exposed region where the oxide is etched and interacts with the thermal Rb atoms. (b) Energy levels of the ladder transition. (c) Schematic description of the device geometry and the measurement setup. Two laser beams at different inputs are focused by a lensed fiber, coupled to the ACWG, propagate through a serpentine shape waveguide, and are collected by another lensed fiber to a detector. The 780 nm reflection from the facets is filtered by a bandpass filter (BPF) (d) photograph of the ACWG chip with an 8−32 Cap Screw for comparison. (e) Measured light transmission through the device at 1529 nm wavelength as a function of the telecom laser detuning for different values of pump power at 780 nm.

enables the fabrication of an entire optical setup including lasers, modulators, and sensors on a chip, reducing the size and cost of such systems. Furthermore, the ACWG supports the propagation of a tightly confined optical mode that allows the observation of nonlinear effects at low optical powers.[36,40−42] The tightly confined light also supports a special type of a circularly polarized mode,[43] and this was used to demonstrate an ACWG-based optical isolator.[44]

Silicon photonics technology was developed for telecommunication and as such operates at the Telcom regime. In contrast, Rb and Cs main optical transitions are at 780 and 852 nm, respectively, there are some molecules such as acetylene and hydrogen cyanide (HCN) that have many transitions in the telecom regime and thus can be used as telecom frequency references and telecom wavelength calibration.[45] Acetylene molecules have also been integrated with hollow-core fibers[46,47] and waveguides[48] to facilitate portable frequency references. Yet, there is great merit in using alkali vapors for frequency reference applications, primarily due to their high dipole strength, narrow transition lines, and superior accuracy. While the most popular transitions of Rb are in the near-infrared (780 and 795 nm), it also has two ladder transitions in the telecom regime,[49,50] which have allowed the stabilization of a laser down to the 1×10^{-11} level[49] as well as all-optical modulation.[51] By locking a frequency comb[52] or a microring-resonator (MRR)[53] to such stable transitions, their stability can be transferred to other telecom wavelengths and generate a grid of frequency references.

In this work, we provide a fast and efficient link between atomic-based devices and telecom components. We do so by using the Rb ladder ($5S_{1/2}$−$5P_{3/2}$−$4D_{5/2}$) transition, with the atom being coupled to a 4 cm long silicon nitride (Si_3N_4) serpentine waveguide. By stabilizing a telecom laser to this transition, we demonstrate a frequency reference with a frequency stability of 9×10^{-10} level at ∼250 s. Following, by exploiting the fast dynamics of the atomic vapor that is interacting with the nanoscale waveguides, we show fast and low power (few nW) all-optical modulation by transferring a telecom signal at a modulation frequency of up to 200 MHz to a 780 nm signal. The fast response and low modulation power enable few photons (up to 24 photons) switching between on and off states. Our device can be used as a miniaturized, chip-scale integrated frequency reference for telecom-based communication and metrology as well as for converting data from integrated atomic-based devices to silicon photonics systems.

■ ACWG PLATFORM

Our ACWG platform is schematically illustrated in Figure. 1a. The device consists of a Si_3N_4 core waveguide on top of a 2 μm thick SiO_2 layer grown on silicon. The waveguide cross-section has a width of 1.5 μm and a height of 0.25 μm, and it is defined by e-beam lithography and reactive ion etching. The waveguide is covered with a 2 μm thick SiO_2 layer as an upper cladding. Within a predefined area, the oxide is removed by buffered hydrofluoric acid (HF) wet etch to create an interaction region between the atomic vapor and the optical mode. In order to improve our ability to observe ladder transitions (Figure 1b), we increase the optical density while maintaining device compactness by constructing a long (40 mm) waveguide in a serpentine-shaped geometry (Figure 1c). Finally, a glass cap is glued to the chip and the device is evacuated, filled with natural rubidium, and pinched off. The result of this process is a portable and hybrid atomic−photonic device that can be seen in Figure 1d. The fabrication process is illustrated in the Supporting Information.

https://dx.doi.org/10.1021/acsphotonics.0c01895
ACS Photonics XXXX, XXX, XXX−XXX

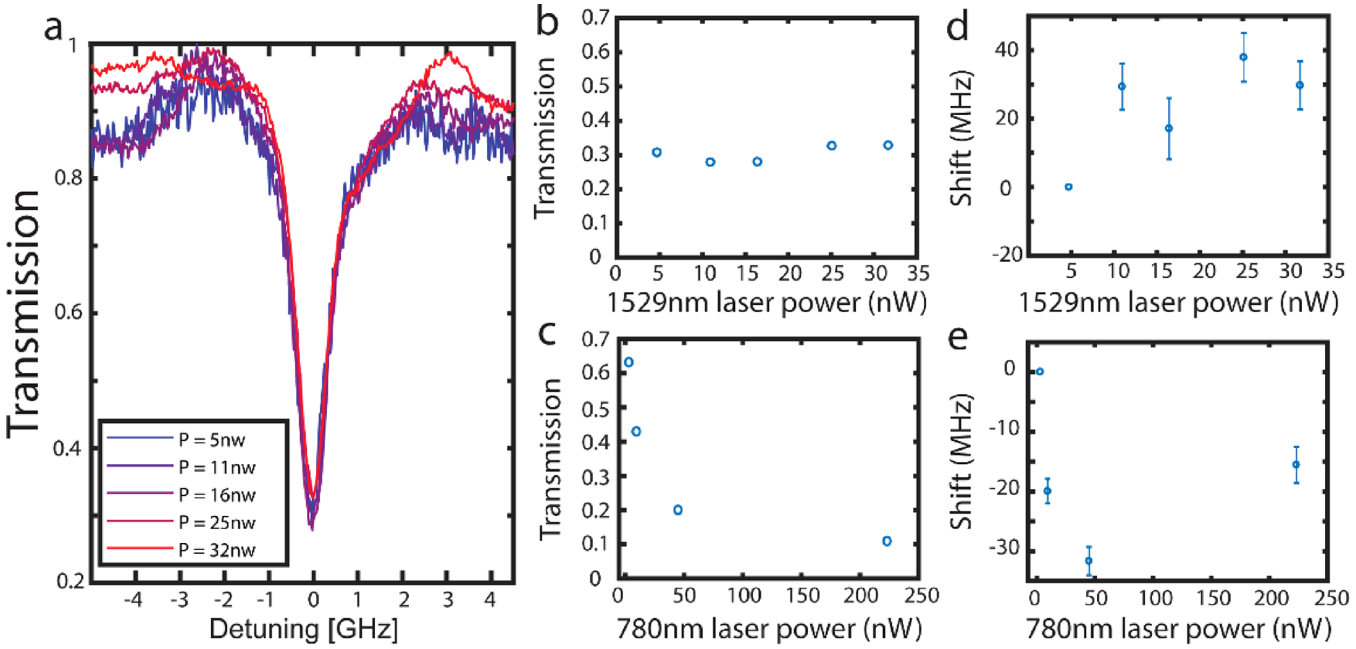

Figure 2. (a) Device transmission at telecom as a function of telecom laser detuning at different telecom laser powers. (b) Telecom transmission on resonance as a function of the telecom laser probe power at pump power of 18 nW. (c) Telecom transmission on resonance as a function of the 780 nm laser pump power at a probe power of 50 nW. (d) The light shift of the telecom transition as a function of the telecom laser probe power at pump power of 18 nW. (e) The light shift of the telecom transition as a function of the 780 nm laser pump power at probe power of 50 nW. Error bar represents the Lorentzian fit uncertainty with 95% confidence.

RESULTS

In Figure 1e, we plot the measured transmission of the light probe through our device at the telecom wavelength of 1529 nm, as we detune its frequency, for several values of pump power at 780 nm. The telecom laser is coupled to the waveguide using a lensed fiber, counter-propagating the 780 nm guided wave, and its transmission through the device is measured by collecting the signal using another lensed fiber that is connected to an InGaAs photodetector. The residual 780 nm reflection, originating predominately from the waveguide facet is filtered out using a bandpass filter (Figure 1c). The two lensed fibers are connected to fiber splitters in order to couple and measure light at each port (Figure 1c). The lensed fibers couple light to the ACWG through inverse tapers and are aligned by precision stages. The coupling losses of our inverse tapers are estimated to be ∼5−10 dB per facet. Input to output losses were measured as 50 dB and are attributed to the coupling losses, bending losses, propagation losses, and fabrication imperfections. The power of the telecom probe within the waveguide is about 50 nw and the 780 nm pump powers are denoted in the legend of the figure. The 780 nm laser is locked to the $F = 3 \rightarrow F' = 4$ transition (Figure 1b) using a separate cm-scale sized Rb cell, and the sample was heated to about 90 °C. As can be seen in Figure 1e, when we use the 1529 nm laser as a probe, it cannot be absorbed in the sample as long as the 780 nm pump is not activated. This is because the $F' = 4$ level is not populated. However, with the increase in pump power, the $F' = 4$ level becomes populated. Now, when the 1529 nm laser is tuned to the $F' = 4 \rightarrow F''$ transition, it can interact with the Rb vapor, because the intermediate level is populated, and the photon energy of the 1529 nm probe photon matches the energy needed to excite an atom from the F' to the F'' level manifold. As a result, a distinct absorption of the 1529 nm probe is observed at resonance. Owing to the use of the long swirl waveguide, we have obtained an absorption in the telecom regime of up to 90%. Due to the nature of the pump−probe experiment, in which the 780 nm laser selects a group of atoms with a specific velocity, one would expect a reduction in the Doppler broadening effect. And indeed, while the Doppler broadened line width in previously demonstrated ACWGs is approximately 1 GHz,[36] our ∼500 MHz broad line (corresponding to a pump power of 3 nW) depicted in Figure 1e represents a significant reduction in the Doppler broadening effect. The observed line width is attributed to other broadening mechanisms, primarily transit time broadening (TTB) and power broadening. In our device, the evanescent decay length of the optical mode is about ∼200 nm, leading to a short interaction time between the photons and the atoms. This gives rise to a significant TTB of about 300 MHz.[36] The additional increase in line width is attributed to power broadening. This can be easily observed from Figure 1e, showing an increase in line width as the pump power is increased. To better understand the spectrum of the transmitted signal and to support our measured results, we have also performed computer simulations (see Supporting Information), which were qualitatively found in good agreement with our measurements.

Next, we aim to stabilize a telecom laser to the atomic transition. In order to do so, we optimize the operation conditions and, in particular, the choice of pump and probe power. As a guideline for such a choice, we recall that, in shot-noise limited systems, the normalized frequency instability ($\Delta f/f$) can be described by the following expression: $\Delta f/f = 0.2/(\mathrm{SNR}\cdot Q)\cdot\tau^{-0.5}$,[54,55] where SNR is the signal-to-noise ratio, Q is the quality (Q) factor, and τ is the integration time. In order to minimize the instability, we should increase the signal, reduce the noise, and increase the Q factor (i.e., reduce the line width). In Figure 2a we plot the absorption in the telecom

https://dx.doi.org/10.1021/acsphotonics.0c01895
ACS Photonics XXXX, XXX, XXX−XXX

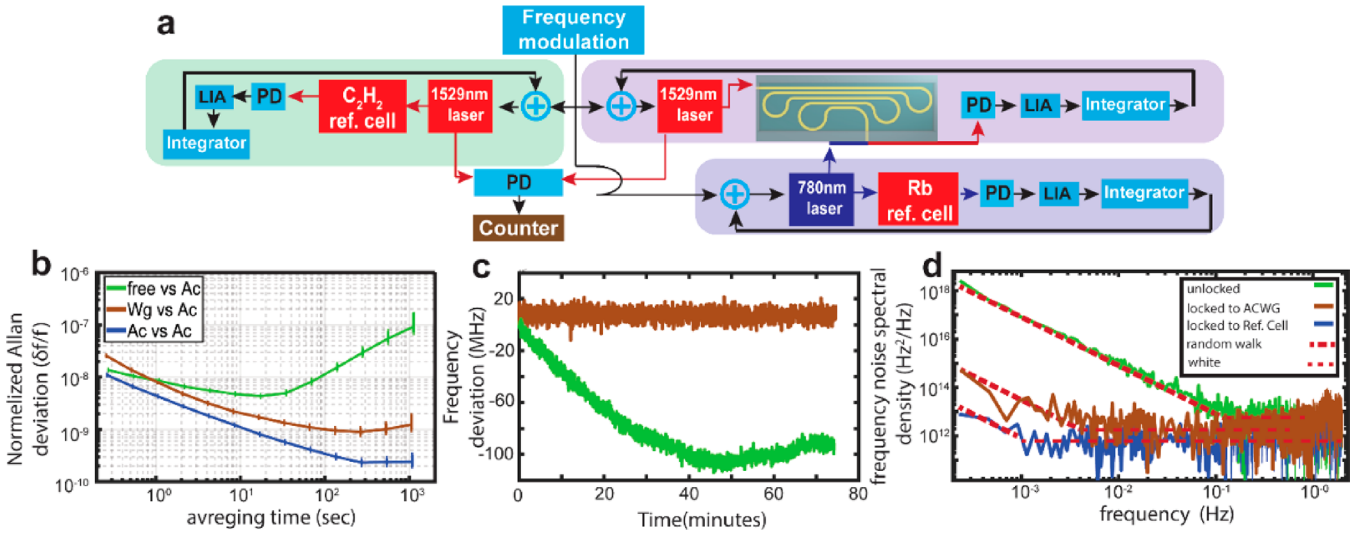

Figure 3. (a) Locking scheme: lasers at 1550 nm are locked to two absorption lines, one from an acetylene reference cell and the other from our ACWG. The 780 nm laser is locked to a Doppler broadened line of a rubidium cm-scale reference cell. The heterodyne beat between the two lasers is fed into a counter, which charts the frequency as a function of time. LIA-lock-in amplifier, PD-photo detector. (b) Allan deviation extracted from the beating between a laser locked to a reference cell and to the free-running laser (green), laser locked to another reference cell (blue), and laser locked to our ACWG (brown). (c) Time series of the frequency of the laser for the unlocked (green) and locked (brown) laser. (d) Frequency noise spectral density of free-running laser (green), laser locked to another reference cell (blue), and laser locked to our ACWG (brown). The dashed lines represent the different noise regions.

regime as a function of the probe power at pump power of 18 nW and observe a very flat response to probe power variation (see Figure 2b). This is because we are below saturation. Saturation will occur when the density of atoms in the top level is close to the amount in the intermediate level. This is expected to happen at higher probe powers. On the other hand, as was shown in Figure 1e, increasing the pump power from 3 to 223 nW increases the absorption by a factor of ∼2 (Figure 2c) at the expense of line width broadening by a factor of ∼3 (see Figure 1e). Furthermore, the high intensity of light within the nanoscale confined mode is expected to give rise to light shifts, manifested in the translation of a power fluctuation to frequency fluctuation, limiting the stability of our system. To investigate this effect, we have fitted the telecom ACWGs transmission under different pump and probe powers to a Lorentzian shape and found the shift as a function of power in respect to the lowest power in the waveguide. In Figure 2d, we plot the shift as a function of the telecom laser probe power. As can be seen, around 30 nW of probe power, the shift is nearly invariant to power variation, making the system more stable. Increasing the current generated in the detector will increase the SNR and reduce the instability. Yet, in our current measurement scheme, we were unable to couple high power due to the combination of losses in the device and the fiber splitters. Due to all the above, we have chosen this value of probe power for the purpose of locking. In Figure 2e we plot the shift as a function of the 780 nm laser power. As shown, for relatively low powers up to about 50 nW, there is a negative shift that is rapidly increasing (in absolute value) as a function of power. Above ∼50 nW we identify a change in the trend, and the shift is gradually reducing with the increase in power. The transition position is determined by the absorption signal, but also by mode interference.[56] This is discussed in more detail in the Supporting Information. For the purpose of locking our system on a stable line, we have chosen 60 nW of pump power as a good compromise between stability and line width.

The locking scheme is presented in Figure 3a, where one tunable laser at telecom wavelength was locked by a wavelength modulation scheme to an absorption signature of an acetylene reference cell, and the other laser was locked to the 1529 nm absorption signature from our ACWG. The pump laser at 780 nm was stabilized using a Doppler broadened absorption signature from a rubidium reference cell at a temperature of ∼25 °C. The 780 nm laser needs to be stabilized in the ladder configuration[49,57] due to the fact that a shift in the 780 nm laser frequency will result in a shift in the 1529 nm absorption signal. This is because the velocity of the atoms that undergo the D2 transition is correlated to the frequency shift of the 780 nm laser, and the same atoms result in a shift in the stabilization of the telecom laser. While in the current demonstration our 780 nm laser was locked to an external cell, our vision is to implement both 780 and 1529 nm locking on the same chip. This will be mitigated in future work. We have measured the beat signal between the two telecom lasers and extracted the instability by an Allan deviation analysis. For comparison, we have also measured the beat signal between two lasers locked to acetylene reference cells and the beat signal between a laser locked to an acetylene reference cell and a free-running laser. The Allan deviation results are depicted in Figure 3b. The result shows laser stabilization to the level of 9×10^{-10} at 263 s. As can be seen, this result is significantly better than the stability of our free-running laser, which has a frequency drift of more than 100 MHz per hour (Figure 3c). The obtained stability is already sufficient for telecom applications that require frequency drifts on the MHz scale and lower.[58−62] While laser drift penalties in communications can be overcome by signal processing, injection locking, or optical phase-lock loops, our chip-scale device offers a simple solution to this issue. The stability achieved here with a compact device can also be useful for outdoor metrological systems.[28] We have analyzed the frequency noise of our system (Figure 3d), and indeed, we are observing a large reduction in random walk noise in the

https://dx.doi.org/10.1021/acsphotonics.0c01895
ACS Photonics XXXX, XXX, XXX−XXX

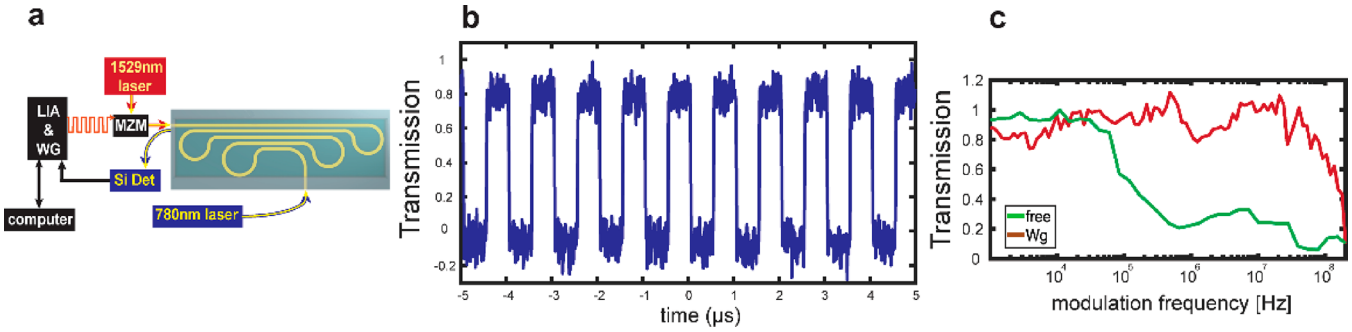

Figure 4. (a) Measurement setup for the all-optical modulation experiment: the telecom laser beam is modulated by a Mach−Zehnder modulator (MZM) and coupled by a lensed fiber to the ACWG. The 780 nm laser beam is coupled by another lensed fiber to the ACWG from the opposite side and propagates through a serpentine shape waveguide. It is coupled to the same lensed fiber that is used for the 1529 nm beam and collected to a silicon photodetector. The signal from the photodetector is fed to a fast lock-in amplifier that serves as a waveform generator as well. (b) Time trace of the 780 nm signal that is modulated by the telecom laser at 1 MHz frequency and 30 nW of power. (c) The frequency response of the 780 nm signal propagating through a free space vapor cell (green) and the ACWG (red).

laser stabilized to the ACWG compared to the free-running laser. At time scales of seconds (higher frequencies), we can see that the precision of our laser is limited by white frequency noise. The current generated in the detector was 5 pA, and it has a bandwidth of 750 Hz, implying a shot noise related SNR of ∼150, whereas the Q factor of the absorption signal is 2×10^5. Using these values, the instability is calculated to be $6.8 \times 10^{-9}\cdot\tau^{-0.5}$ for white noise limited systems. Indeed, this result is very similar to our measured instability at the white noise limited region. We modulate our laser frequency at a deviation of ∼10 MHz with a frequency of ∼700 Hz; this results in an additional instability of $0.2 \times 10^{-9}\cdot\tau^{-0.5}$, significantly lower than the white noise limit. At short integration times of less than 1 s, the Allan deviation and the noise spectrum deviate from white noise behavior. The instability obtained with our ACWG device is only less than an order of magnitude inferior as compared to the instability obtained with the large reference cell. Currently, the obtained instability still falls short, with values reported for large free space systems.[49,52] This is mostly due to factors such as intensity fluctuations, temperature fluctuations, and broadening mechanisms. A detailed discussion regarding the sources of instability and the mitigation approaches is provided in the Supporting Information. While our current instability is about 2 orders of magnitude higher than that achieved with large cells,[49] our device is more than 6 orders of magnitude smaller in volume. Defining the figure of merit as 1/(size times instability), our device is orders of magnitude superior as compared to free space systems. Yet size is not the only benefit, this chip-scale device could be implemented alongside on-chip electronics,[63] lasers,[64] modulators,[15] and detectors,[10] enabling a full on-chip locking system. The important advantage of integrating atoms on a chip is in bringing long time stability and accuracy to chip-scale devices. We show here instability of better than 250 kHz at 1000 s. While not measured against an optical atomic clock, our system is expected to provide decent accuracy without the need for calibration, because it is based on an atomic reference. In contrast, integrated resonators do not possess the accuracy and the long-term stability that atoms provide. In fact, such devices need to be tuned[65] or locked[53] in order to reach a specific spectral position. At short time scales, millimeter size resonators can reach a high precision manifested by very low instability (10^{-13}),[66,67] but at longer integration times, temperature fluctuations are expected to deteriorate the stability of the system. As an example, in the case of MRR, we have shown that instability is increased from 1 to 20 MHz already at 1000 s.[53] Thermal isolation and stabilization, for example, by using the frequency shift between two modes in a millimeter scale resonator in a vacuum chamber can result in long-term stability (10^{-10}, 1000 s).[68] Yet, the device still needs to be calibrated to a known atomic transition. As such, the ACWG offers laser stabilization with low long-term stability at an atomic deterministic frequency using an integrated and miniaturized chip-scale device.

The fast dynamics of the atoms passing through the nanoscale evanescent interaction region enables fast and efficient all-optical modulation. In a case of a large, cm-scale ref cell with a millimeter size laser beam waist, an atom will reside in an excited level for about 26 ns for the case of the 780 nm beam and 84 ns in the case of the 1529 nm beam. As a result, the modulation bandwidth is limited to a few MHz. In contrast, within our ACWG device, an atom will interact with the ∼100 nm evanescent field for less than 5 ns, increasing the transit time broadening that in turn increases the bandwidth. This is one rare example in which larger atomic line width plays a positive role. In order to demonstrate this ability, we have modulated our telecom laser and measured the response at the 780 nm wavelength. The 780 nm power inside the waveguide was ∼200 nW, and the modulated telecom signal was at ∼30 nW. First, we used a Mach−Zehnder modulator (MZM) to modulate the telecom laser with a rectangular waveform and used an oscilloscope to capture the output from the ACWG with a fast Si detector (Figure 4a). In Figure 4b we can see the undistorted output of a 1 MHz rectangular wave, demonstrating the all-optical modulation capability. In order to characterize the frequency response of the all-optical modulation scheme within our ACWG, we have used a high-frequency lock-in amplifier (LIA) while sweeping the modulation frequency and recording its output. We have measured the frequency response both for the ACWG system and for a conventional free-space vapor cell heated to 70 C. In Figure 4c we present the frequency response of both the ACWG system and the free-space system. As can be observed, while the free space system is limited to about 100 kHz, our ACWG operates up to 200 MHz. This is due to the additional broadening mechanisms in our ACWG, as discussed in the previous sections. Thus, while broadening is considered as a negative effect for precision metrology applications, it is

https://dx.doi.org/10.1021/acsphotonics.0c01895
ACS Photonics XXXX, XXX, XXX−XXX

actually beneficial for other applications in which large bandwidth is needed, such as high-speed modulation. Furthermore, the fast response combined with a low modulation power of the telecom laser (~6 nW; telecom) results in very low switching energies, corresponding to only ~100 photons that are needed to perform the switching. We determine the switching energy as the telecom power needed to generate a peak in the 780 nm absorption spectrum, which is 6 nW. This result is presented in the Supporting Information. The time response equivalent to a bandwidth of 200 MHz is ~2 ns ($t = 0.34/\mathrm{BW}$). The optical energy is 6 nW·2 ns = 12×10^{-18} J, corresponding to $2 \times 10^{-18}/1.3 \times 10^{-19}$ = 92 photons. We can also consider the other alternative, where we switch between the pump and the probe and use the modulation of the 780 nm laser to modulate the telecom signal. As shown in Figure 1e, such modulation can be performed efficiently with power levels as low as 3 nW for the 780 nm laser. Thus, we can estimate the required number of photons for such a modulation to be ~25. These highly efficient modulation schemes benefit from the chip-scale integration and the nanoscale confinement of the ACWG. This efficient transduction can be useful in many ways; we can propagate, filter, and modulate a telecom signal, convert it to 780 nm, and pass it to an atomic-based device. We can also take the output of an atomic-based device and directly convert it to a telecom signal that could propagate several kilometers on a standard fiber. Furthermore, detecting telecom photons on a chip requires more complex solutions, such as Schottky detectors[69] and semiconductor heterostructures;[11,12] by converting telecom photons to 780 nm photons, we can overcome this issue and use a standard Si photodetector.

In summary, we have constructed a 4 cm long ACWG in a serpentine-like geometry with the purpose of providing a chip-scale platform to bridge between transitions of alkali vapors in the near-infrared and the telecom spectral regime. Specifically, we have used this platform to demonstrate a highly compact telecom-based atomic optical frequency reference, as well as efficient and fast telecom-near IR all-optical switching. Based on the ladder transition in an atomic cladded rubidium vapor waveguide, we were able to achieve a high contrast absorption signal in the telecom band. This absorption signal was controlled all-optically using only a few nW of power of the 780 nm pump laser. We have used this absorption signal to stabilize a telecom laser to less than 200 kHz and analyzed the frequency dependence of the line shape as a function of pump and probe power. Additionally, we have exploited the broadening mechanisms of our ACWG for the benefit of performing fast all-optical modulation with a frequency response of up to 200 MHz.

Our ACWG platform, combined with the atomic ladder transition, brings the chip-scale alkali vapor science and technology closer into the telecom regime. In the future, by integrating this chip-scale device with on-chip electronics, photodetectors, and perhaps even light sources, we envision the construction of fully integrated chip-scale atomic systems for diverse applications ranging from stabilized laser sources and frequency references to magnetometry and all-optical switching down to a few photons and even the single-photon level. Furthermore, the ability to translate between the telecom and the near-IR regime makes our ACWG approach attractive for integration with the platform of silicon photonics, with the goal of constructing low power nonlinear devices for chip-scale quantum applications.

■ ASSOCIATED CONTENT

Supporting Information

The Supporting Information is available free of charge at https://pubs.acs.org/doi/10.1021/acsphotonics.0c01895.

Calculation of rubidium transition susceptibility in the evanescent region, calculation of absorption for ladder measurement, measured transmission at 780 nm as a function of the pump (1529 nm) detuning and power, simulation of the device transmission under variations in absorption and temperature, and the fabrication process (PDF)

■ AUTHOR INFORMATION

Corresponding Author

Uriel Levy − *Department of Applied Physics, The Benin School of Engineering and Computer Science, The Center for Nanoscience and Nanotechnology, The Hebrew University of Jerusalem, Jerusalem 91904, Israel;* orcid.org/0000-0002-5918-1876; Email: ulevy@mail.huji.ac.il

Authors

Roy Zektzer − *Department of Applied Physics, The Benin School of Engineering and Computer Science, The Center for Nanoscience and Nanotechnology, The Hebrew University of Jerusalem, Jerusalem 91904, Israel;* orcid.org/0000-0003-2751-7379

Eliran Talker − *Department of Applied Physics, The Benin School of Engineering and Computer Science, The Center for Nanoscience and Nanotechnology, The Hebrew University of Jerusalem, Jerusalem 91904, Israel*

Yefim Barash − *Department of Applied Physics, The Benin School of Engineering and Computer Science, The Center for Nanoscience and Nanotechnology, The Hebrew University of Jerusalem, Jerusalem 91904, Israel*

Noa Mazurski − *Department of Applied Physics, The Benin School of Engineering and Computer Science, The Center for Nanoscience and Nanotechnology, The Hebrew University of Jerusalem, Jerusalem 91904, Israel*

Liron Stern − *Department of Applied Physics, The Benin School of Engineering and Computer Science, The Center for Nanoscience and Nanotechnology, The Hebrew University of Jerusalem, Jerusalem 91904, Israel;* orcid.org/0000-0002-4588-110X

Complete contact information is available at: https://pubs.acs.org/10.1021/acsphotonics.0c01895

Funding

The research was supported by the Israeli Science Foundation (ISF) and by the Israeli Ministry of Science and Technology.

Notes

The authors declare no competing financial interest.

■ REFERENCES

(1) Soref, R.; Larenzo, J. All-Silicon Active and Passive Guided-Wave Components for $\lambda = 1.3$ and 1.6 Mm. *IEEE J. Quantum Electron.* **1986**, *22* (6), 873−879.

(2) Luo, L.-W.; Ophir, N.; Chen, C. P.; Gabrielli, L. H.; Poitras, C. B.; Bergmen, K.; Lipson, M. WDM-Compatible Mode-Division Multiplexing on a Silicon Chip. *Nat. Commun.* **2014**, *5* (1), 3069.

(3) Shacham, A.; Bergman, K.; Carloni, L. P. Photonic Networks-on-Chip for Future Generations of Chip Multiprocessors. *IEEE Trans. Comput.* **2008**, *57* (9), 1246−1260.

(4) Cheng, Q.; Bahadori, M.; Glick, M.; Rumley, S.; Bergman, K. Recent Advances in Optical Technologies for Data Centers: A Review. *Optica* **2018**, *5* (11), 1354.
(5) Rickman, A. The Commercialization of Silicon Photonics. *Nat. Photonics* **2014**, *8* (8), 579−582.
(6) Naiman, A.; Desiatov, B.; Stern, L.; Mazurski, N.; Shappir, J.; Levy, U. Ultrahigh-Q Silicon Resonators in a Planarized Local Oxidation of Silicon Platform. *Opt. Lett.* **2015**, *40* (9), 1892.
(7) Pfeiffer, M. H. P.; Liu, J.; Raja, A. S.; Morais, T.; Ghadiani, B.; Kippenberg, T. J. Ultra-Smooth Silicon Nitride Waveguides Based on the Damascene Reflow Process: Fabrication and Loss Origins. *Optica* **2018**, *5* (7), 884.
(8) Ji, X.; Barbosa, F. A. S.; Roberts, S. P.; Dutt, A.; Cardenas, J.; Okawachi, Y.; Bryant, A.; Gaeta, A. L.; Lipson, M. Ultra-Low-Loss on-Chip Resonators with Sub-Milliwatt Parametric Oscillation Threshold. *Optica* **2017**, *4* (6), 619.
(9) Nezhad, M. P.; Bondarenko, O.; Khajavikhan, M.; Simic, A.; Fainman, Y. Etch-Free Low Loss Silicon Waveguides Using Hydrogen Silsesquioxane Oxidation Masks. *Opt. Express* **2011**, *19* (20), 18827.
(10) Goykhman, I.; Desiatov, B.; Khurgin, J.; Shappir, J.; Levy, U. Locally Oxidized Silicon Surface-Plasmon Schottky Detector for Telecom Regime. *Nano Lett.* **2011**, *11* (6), 2219−2224.
(11) Chen, L.; Lipson, M. Ultra-Low Capacitance and High Speed Germanium Photodetectors on Silicon. *Opt. Express* **2009**, *17* (10), 7901.
(12) Park, H.; Fang, A. W.; Jones, R.; Cohen, O.; Raday, O.; Sysak, M. N.; Paniccia, M. J.; Bowers, J. E. A Hybrid AlGaInAs-Silicon Evanescent Waveguide Photodetector. *Opt. Express* **2007**, *15* (10), 6044.
(13) Goykhman, I.; Desiatov, B.; Ben-Ezra, S.; Shappir, J.; Levy, U. Optimization of Efficiency-Loss Figure of Merit in Carrier-Depletion Silicon Mach-Zehnder Optical Modulator. *Opt. Express* **2013**, *21* (17), 19518−19529.
(14) Sorianello, V.; Midrio, M.; Contestabile, G.; Asselberghs, I.; Van Campenhout, J.; Huyghebaert, C.; Goykhman, I.; Ott, A. K.; Ferrari, A. C.; Romagnoli, M. Graphene-Silicon Phase Modulators with Gigahertz Bandwidth. *Nat. Photonics* **2018**, *12* (1), 40−44.
(15) Xu, Q.; Schmidt, B.; Pradhan, S.; Lipson, M. Micrometre-Scale Silicon Electro-Optic Modulator. *Nature* **2005**, *435* (7040), 325−327.
(16) Thomson, D. J.; Gardes, F. Y.; Fedeli, J.-M.; Zlatanovic, S.; Hu, Y.; Kuo, B. P. P.; Myslivets, E.; Alic, N.; Radic, S.; Mashanovich, G. Z.; et al. 50-Gb/s Silicon Optical Modulator. *IEEE Photonics Technol. Lett.* **2012**, *24* (4), 234−236.
(17) Piggott, A. Y.; Lu, J.; Lagoudakis, K. G.; Petykiewicz, J.; Babinec, T. M.; Vučković, J. Inverse Design and Demonstration of a Compact and Broadband On-Chip Wavelength Demultiplexer. *Nat. Photonics* **2015**, *9* (6), 374−377.
(18) Ohana, D.; Desiatov, B.; Mazurski, N.; Levy, U. Dielectric Metasurface as a Platform for Spatial Mode Conversion in Nanoscale Waveguides. *Nano Lett.* **2016**, *16* (12), 7956−7961.
(19) Stern, L.; Naiman, A.; Keinan, G.; Mazurski, N.; Grajower, M.; Levy, U. Ultra-Precise Optical to Radio Frequency Based Chip-Scale Refractive Index and Temperature Sensor. *Optica* **2017**, *4* (1), 1.
(20) Lee, H.; Suh, M.-G.; Chen, T.; Li, J.; Diddams, S. A.; Vahala, K. J. Spiral Resonators for On-Chip Laser Frequency Stabilization. *Nat. Commun.* **2013**, *4* (1), 2468.
(21) Naiman, A.; Stern, L.; Levy, U. On-Chip Beam Positioning Sensor via Frequency Locked Cascaded Ring Resonators. *Appl. Phys. Lett.* **2018**, *112* (20), 201112.
(22) Srinivasan, S.; Moreira, R.; Blumenthal, D.; Bowers, J. E. Design of Integrated Hybrid Silicon Waveguide Optical Gyroscope. *Opt. Express* **2014**, *22* (21), 24988.
(23) Lai, Y.-H.; Suh, M.-G.; Lu, Y.-K.; Shen, B.; Yang, Q.-F.; Wang, H.; Li, J.; Lee, S. H.; Yang, K. Y.; Vahala, K. Earth Rotation Measured by a Chip-Scale Ring Laser Gyroscope. *Nat. Photonics* **2020**, *14* (6), 345−349.
(24) Newman, Z. L.; Maurice, V.; Drake, T.; Stone, J. R.; Briles, T. C.; Spencer, D. T.; Fredrick, C.; Li, Q.; Westly, D.; Ilic, B. R.; et al. Architecture for the Photonic Integration of an Optical Atomic Clock. *Optica* **2019**, *6* (5), 680.
(25) Papp, S. B.; Beha, K.; Del'Haye, P.; Quinlan, F.; Lee, H.; Vahala, K. J.; Diddams, S. a. Microresonator Frequency Comb Optical Clock. *Optica* **2014**, *1* (1), 10.
(26) Griffith, A. G.; Lau, R. K. W.; Cardenas, J.; Okawachi, Y.; Mohanty, A.; Fain, R.; Lee, Y. H. D.; Yu, M.; Phare, C. T.; Poitras, C. B.; et al. Silicon-Chip Mid-Infrared Frequency Comb Generation. *Nat. Commun.* **2015**, *6*, 6299.
(27) Pfeifle, J.; Brasch, V.; Lauermann, M.; Yu, Y.; Wegner, D.; Herr, T.; Hartinger, K.; Schindler, P.; Li, J.; Hillerkuss, D.; et al. Coherent Terabit Communications with Microresonator Kerr Frequency Combs. *Nat. Photonics* **2014**, *8* (5), 375−380.
(28) Suh, M.-G.; Yi, X.; Lai, Y.-H.; Leifer, S.; Grudinin, I. S.; Vasisht, G.; Martin, E. C.; Fitzgerald, M. P.; Doppmann, G.; Wang, J.; et al. Searching for Exoplanets Using a Microresonator Astrocomb. *Nat. Photonics* **2019**, *13* (1), 25−30.
(29) Fülöp, A.; Mazur, M.; Lorences-Riesgo, A.; Helgason, Ó. B.; Wang, P.-H.; Xuan, Y.; Leaird, D. E.; Qi, M.; Andrekson, P. A.; Weiner, A. M.; et al. High-Order Coherent Communications Using Mode-Locked Dark-Pulse Kerr Combs from Microresonators. *Nat. Commun.* **2018**, *9* (1), 1598.
(30) Blumenthal, D. J.; Ballani, H.; Behunin, R. O.; Bowers, J. E.; Costa, P.; Lenoski, D.; Morton, P. A.; Papp, S. B.; Rakich, P. T. Frequency-Stabilized Links for Coherent WDM Fiber Interconnects in the Datacenter. *J. Lightwave Technol.* **2020**, *38* (13), 3376−3386.
(31) Hosseini, M.; Sparkes, B. M.; Campbell, G.; Lam, P. K.; Buchler, B. C. High Efficiency Coherent Optical Memory with Warm Rubidium Vapour. *Nat. Commun.* **2011**, *2* (1), 174−175.
(32) Kominis, I. K.; Kornack, T. W.; Allred, J. C.; Romalis, M. V. A Subfemtotesla Multichannel Atomic Magnetometer. *Nature* **2003**, *422* (6932), 596−599.
(33) Spillane, S. M.; Pati, G. S.; Salit, K.; Hall, M.; Kumar, P.; Beausoleil, R. G.; Shahriar, M. S. Observation of Nonlinear Optical Interactions of Ultralow Levels of Light in a Tapered Optical Nanofiber Embedded in a Hot Rubidium Vapor. *Phys. Rev. Lett.* **2008**, *100* (23), 1−4.
(34) Yang, W.; Conkey, D. B.; Wu, B.; Yin, D.; Hawkins, A. R.; Schmidt, H. Atomic Spectroscopy on a Chip. *Nat. Photonics* **2007**, *1* (6), 331−335.
(35) Knappe, S.; Shah, V.; Schwindt, P. D. D.; Hollberg, L.; Kitching, J.; Liew, L. A.; Moreland, J. A Microfabricated Atomic Clock. *Appl. Phys. Lett.* **2004**, *85* (9), 1460−1462.
(36) Stern, L.; Desiatov, B.; Goykhman, I.; Levy, U. Nanoscale Light-Matter Interactions in Atomic Cladding Waveguides. *Nat. Commun.* **2013**, *4*, 1548.
(37) Stern, L.; Desiatov, B.; Mazurski, N.; Levy, U. Strong Coupling and High-Contrast All-Optical Modulation in Atomic Cladding Waveguides. *Nat. Commun.* **2017**, *8* (1), 14461.
(38) Ritter, R.; Gruhler, N.; Dobbertin, H.; Kübler, H.; Scheel, S.; Pernice, W.; Pfau, T.; Löw, R. Coupling Thermal Atomic Vapor to Slot Waveguides. *Phys. Rev. X* **2018**, *8* (2), 021032.
(39) Ritter, R.; Gruhler, N.; Pernice, W.; Kübler, H.; Pfau, T.; Löw, R. Atomic Vapor Spectroscopy in Integrated Photonic Structures. *Appl. Phys. Lett.* **2015**, *107* (4), 041101.
(40) Stern, L.; Zektzer, R.; Mazurski, N.; Levy, U. Enhanced Light-Vapor Interactions and All Optical Switching in a Chip Scale Micro-Ring Resonator Coupled with Atomic Vapor. *Laser photonics Rev.* **2016**, *10* (6), 1016−1022.
(41) Talker, E.; Arora, P.; Barash, Y.; Stern, L.; Levy, U. Plasmonic Enhanced EIT and Velocity Selective Optical Pumping Measurements with Atomic Vapor. *ACS Photonics* **2018**, *5* (7), 2609−2616.
(42) Skljarow, A.; Gruhler, N.; Pernice, W.; Kübler, H.; Pfau, T.; Löw, R.; Alaeian, H. Integrating Two-Photon Nonlinear Spectroscopy of Rubidium Atoms with Silicon Photonics. *Opt. Express* **2020**, *28* (13), 19593.
(43) Stern, L.; Grajower, M.; Mazurski, N.; Levy, U. Magnetically Controlled Atomic - Plasmonic Fano Resonances. *Nano Lett.* **2018**, *18* (1), 202−207.

https://dx.doi.org/10.1021/acsphotonics.0c01895
ACS Photonics XXXX, XXX, XXX−XXX

(44) Zektzer, R.; Talker, E.; Barash, Y.; Mazurski, N.; Levy, U. Chiral Light-Matter Interactions in Hot Vapor-Cladded Waveguides. *Optica* **2019**, *6* (1), 15.
(45) Gilbert, S. L.; Swann, W. C. Acetylene $^{12}C_2H_2$ Absorption Reference for 1510 Nm to 1540 Nm Wavelength Calibration−SRM 2517a. *Nist Spec. Publ., Report No. 260-133*, 2001.
(46) Knabe, K.; Wu, S.; Lim, J.; Tillman, K. A.; Light, P. S.; Couny, F.; Wheeler, N.; Thapa, R.; Jones, A. M.; Nicholson, J. W.; et al. 10 kHz Accuracy of an Optical Frequency Reference Based on 12C_2H_2-Filled Large-Core Kagome Photonic Crystal Fibers. *Opt. Express* **2009**, *17* (18), 16017.
(47) Wang, C.; Wheeler, N. V.; Fourcade-Dutin, C.; Grogan, M.; Bradley, T. D.; Washburn, B. R.; Benabid, F.; Corwin, K. L. Acetylene Frequency References in Gas-Filled Hollow Optical Fiber and Photonic Microcells. *Appl. Opt.* **2013**, *52* (22), 5430.
(48) Zektzer, R.; Hummon, M. T.; Stern, L.; Sebbag, Y.; Barash, Y.; Mazurski, N.; Kitching, J.; Levy, U. A Chip-Scale Optical Frequency Reference for the Telecommunication Band Based on Acetylene. *Laser Photonics Rev.* **2020**, *14* (6), 1900414.
(49) Moon, H. S.; Lee, W. K.; Lee, L.; Kim, J. B. Double Resonance Optical Pumping Spectrum and Its Application for Frequency Stabilization of a Laser Diode. *Appl. Phys. Lett.* **2004**, *85* (18), 3965−3967.
(50) Talker, E.; Stern, L.; Naiman, A.; Barash, Y.; Levy, U. Fluorescence Double Resonance Optical Pumping Spectrum and Its Application for Frequency Stabilization in Millimeter Scale Vapor Cells. *J. Phys. Commun.* **2017**, *1* (5), 055016.
(51) Krishnamurthy, S.; Wang, Y.; Tu, Y.; Tseng, S.; Shahriar, M. S. High Efficiency Optical Modulation at a Telecom Wavelength Using the Quantum Zeno Effect in a Ladder Transition in Rb Atoms. *Opt. Express* **2012**, *20* (13), 13798−13809.
(52) Stern, L.; Stone, J. R.; Kang, S.; Cole, D. C.; Suh, M.-G.; Fredrick, C.; Newman, Z.; Vahala, K.; Kitching, J.; Diddams, S. A.; et al. Direct Kerr Frequency Comb Atomic Spectroscopy and Stabilization. *Sci. Adv.* **2020**, *6* (9), No. eaax6230.
(53) Zektzer, R.; Stern, L.; Mazurski, N.; Levy, U. On-Chip Multi Spectral Frequency Standard Replication by Stabilizing a Microring Resonator to a Molecular Line. *Appl. Phys. Lett.* **2016**, *109* (1), 10−14.
(54) Vanier, J.; Mandache, C. The Passive Optically Pumped Rb Frequency Standard: The Laser Approach. *Appl. Phys. B: Lasers Opt.* **2007**, *87* (4), 565−593.
(55) Drever, R. W. P.; Hall, J. L.; Kowalski, F. V.; Hough, J.; Ford, G. M.; Munley, A. J.; Ward, H. Laser Phase and Frequency Stabilization Using an Optical Resonator. *Appl. Phys. B: Photophys. Laser Chem.* **1983**, *31* (2), 97−105.
(56) Zektzer, R.; Stern, L.; Mazurski, N.; Levy, U. Enhanced Light-Matter Interactions in Plasmonic-Molecular Gas Hybrid System. *Optica* **2018**, *5* (4), 486.
(57) Stern, L.; Stone, J. R.; Kang, S.; Cole, D. C.; Suh, M.; Fredrick, C.; Newman, Z.; Vahala, K.; Kitching, J.; Diddams, S. A.; et al. Direct Kerr Frequency Comb Atomic Spectroscopy and Stabilization. *Sci. Adv.* **2020**, *6* (9), No. eaax6230.
(58) Igarashi, K.; Tsuritani, T.; Morita, I.; Katoh, K.; Kikuchi, K. Frequency Stabilization of Multiple Semiconductor Lasers for Nyquist-WDM Transmission Systems. In *Optical Fiber Communication Conference/National Fiber Optic Engineers Conference 2013*; OSA: Washington, D.C., 2013; Vol. 2, p OTu2I.6. DOI: 10.1364/OFC.2013.OTu2I.6.
(59) Ly-Gagnon, D.-S.; Tsukamoto, S.; Katoh, K.; Kikuchi, K. Coherent Detection of Optical Quadrature Phase-Shift Keying Signals with Carrier Phase Estimation. *J. Lightwave Technol.* **2006**, *24* (1), 12−21.
(60) Yamamoto, Y.; Kimura, T. Coherent Optical Fiber Transmission Systems. *IEEE J. Quantum Electron.* **1981**, *17* (6), 919−935.
(61) Soeiro, R. O. J.; Alves, T. M. F.; Cartaxo, A. V. T. Inter-Ring Band-Transfer Limited by Laser Wavelength Drift in DD MB-OFDM Metro Networks. *J. Lightwave Technol.* **2016**, *34* (10), 2473−2483.
(62) Perin, J. K.; Shastri, A.; Kahn, J. M. Design of Low-Power DSP-Free Coherent Receivers for Data Center Links. *J. Lightwave Technol.* **2017**, *35* (21), 4650−4662.
(63) Idjadi, M. H.; Aflatouni, F. Integrated Pound-Drever-Hall Laser Stabilization System in Silicon. *Nat. Commun.* **2017**, *8* (1), 1−9.
(64) Fang, A. W.; Park, H.; Cohen, O.; Jones, R.; Paniccia, M. J.; Bowers, J. E. Electrically Pumped Hybrid AlGaInAs-Silicon Evanescent Laser. *Opt. Express* **2006**, *14* (20), 9203.
(65) Grajower, M.; Mazurski, N.; Shappir, J.; Levy, U. Non-Volatile Silicon Photonics Using Nanoscale Flash Memory Technology. *Laser Photon. Rev.* **2018**, *12* (4), 1700190.
(66) Lee, H.; Suh, M. G.; Chen, T.; Li, J.; Diddams, S. A.; Vahala, K. J. Spiral Resonators for On-Chip Laser Frequency Stabilization. *Nat. Commun.* **2013**, *4*, na.
(67) Zhang, W.; Stern, L.; Carlson, D.; Bopp, D.; Newman, Z.; Kang, S.; Kitching, J.; Papp, S. B. Ultranarrow Linewidth Photonic-Atomic Laser. *Laser Photonics Rev.* **2020**, *14* (4), 1900293.
(68) Baumgartel, L. M.; Thompson, R. J.; Yu, N. Frequency Stability of a Dual-Mode Whispering Gallery Mode Optical Reference Cavity. *Opt. Express* **2012**, *20* (28), 29798.
(69) Goykhman, I.; Desiatov, B.; Khurgin, J.; Shappir, J.; Levy, U. Waveguide Based Compact Silicon Schottky Photodetector with Enhanced Responsivity in the Telecom Spectral Band. *Opt. Express* **2012**, *20* (27), 28594−28602.

https://dx.doi.org/10.1021/acsphotonics.0c01895
ACS Photonics XXXX, XXX, XXX−XXX